



Article

Multiple-Vector Model Predictive Control with Fuzzy Logic for PMSM Electric Drive Systems

Ibrahim Farouk Bouguenna ¹, Ahmed Tahour ², Ralph Kennel ³ and Mohamed Abdelrahem ^{3,4,*}

¹ Institute for Electrical Engineering, University of Mascara, Mascara 29000, Algeria; i.bouguenna@univ-mascara.dz

² Higher School of Applied Sciences, Tlemcen 13000, Algeria; a.tahour@univ-mascara.dz

³ Institute for Electrical Drive Systems and Power Electronics (EAL), Technische Universität München (TUM), 80333 Munich, Germany; ralph.kennel@tum.de

⁴ Electrical Engineering Department, Faculty of Engineering, Assiut University, Assiut 71516, Egypt

* Correspondence: mohamed.abdelrahem@tum.de or mohamed.abdelrahem@aun.edu.eg

Abstract: This article presents a multiple-vector finite-control-set model predictive control (MV-FCS-MPC) scheme with fuzzy logic for permanent-magnet synchronous motors (PMSMs) used in electric drive systems. The proposed technique is based on discrete space vector modulation (DSVM). The converter's real voltage vectors are utilized along with new virtual voltage vectors to form switching sequences for each sampling period in order to improve the steady-state performance. Furthermore, to obtain the reference voltage vector (VV) directly from the reference current and to reduce the calculation load of the proposed MV-FCS-MPC technique, a deadbeat function (DB) is added. Subsequently, the best real or virtual voltage vector to be applied in the next sampling instant is selected based on a certain cost function. Moreover, a fuzzy logic controller is employed in the outer loop for controlling the speed of the rotor. Accordingly, the dynamic response of the speed is improved and the difficulty of the proportional-integral (PI) controller tuning is avoided. The response of the suggested technique is verified by simulation results and compared with that of the conventional FCS-MPC.

Keywords: model predictive control; fuzzy logic controller; multiple-vector; deadbeat function



Citation: Bouguenna, I.F.; Tahour, A.; Kennel, R.; Abdelrahem, M. Multiple-Vector Model Predictive Control with Fuzzy Logic for PMSM Electric Drive Systems. *Energies* **2021**, *14*, 1727. <https://doi.org/10.3390/en14061727>

Academic Editor: Antonino Oscar Di Tommaso

Received: 9 February 2021

Accepted: 16 March 2021

Published: 20 March 2021

Publisher's Note: MDPI stays neutral with regard to jurisdictional claims in published maps and institutional affiliations.



Copyright: © 2021 by the authors. Licensee MDPI, Basel, Switzerland. This article is an open access article distributed under the terms and conditions of the Creative Commons Attribution (CC BY) license (<https://creativecommons.org/licenses/by/4.0/>).

1. Introduction

The growing phenomenon of global warming and transportation-induced air emissions in urban areas has accelerated the introduction of several alternative mobility solutions such as electric vehicles, car sharing, and e-bikes [1]. This electric mobility has several advantages: Electric energy is cheaper and less polluting than oil, the efficiency of an electric motor is higher than an internal combustion engine, the electric vehicle is less noisy, and is rechargeable at home [2,3]. Therefore, it is necessary for the research community to conduct research focused on clean, renewable, and green energy sources and to put pressure on political/economic decision-makers in order to take meaningful action to resolve this challenge and to support the energy transition [4]. In this context, the gradual arrival of electric and hybrid vehicles on a more competitive market than ever, leads car manufacturers to develop ever more efficient vehicles while having lower costs. The performance criteria for electric vehicles are reliability, robustness, power management, speed of charge of the batteries, and especially the electric drive system [5]. To ensure the drive of the electric vehicle, several categories of electric machines exist such as: Direct current machines, asynchronous machines, and synchronous machines. Many researches on electric vehicles have been carried out to enhance its performance [6]. Most of this work has been done on their power sources and structures, and on its electric drive system. Work on the electric drive system was of great interest to car manufacturers and researchers [7].

Permanent magnet synchronous motors (PMSMs) are increasingly becoming strong candidates in several electrical drive systems because of their particular features of having a higher power factor, very good efficiency, excellent torque density, no slip rings (i.e., lower maintenance time and effort), very low rate of failure, and excellent reliability [8,9]. These features and other advantages like fast dynamic performance, developed field weakening techniques, and excellent controllability make the PMSMs the right tool for traction systems such as in electrical/hybrid vehicles [10,11]. Many strategies for PMSM drive control have been suggested including direct torque control (DTC) [12], direct flux control (DFC) technique [13], and field oriented control (FOC) [14]. The FOC system typically uses cascade control loops for speed, position, and torque control with several proportional-integral (PI) controllers [15,16]. The FOC solution was widely used in PMSM control, owing to the benefits of a straightforward technique and good reliability. Nevertheless, the FOC's disadvantages are the cascade mechanism, which reduce the speed of the dynamic performance of the controller [17–20]. The DFC method can be applied to the three-phase synchronous machine with an accessible star-point, which are usually for low power applications. DTC is characterized by a fast dynamic response but it is influenced by a substantial ripple of torque which could then be compensated by other methods [21]. Therefore, these classic methods ignore these facts, affecting the high performance of the PMSM and the whole electrical drive system [22–24]. Currently, thanks to the great development of digital signal processors (DSPs), which enables the application of numerous advanced/non-linear control techniques such as adaptive control, sliding mode control (SMC), predictive control, neuron network control (NNC), and fuzzy logic [23,24] on PMSM drive systems [25].

Predictive control has emerged in recent years as a powerful controller, which applied for numerous applications such as inverters, rectifiers, converters, motors, and others. The basic idea of predictive control is using the system model to anticipate for the control variables the future performance and then achieve optimum action by employing a certain optimization criteria [26]. Predictive control (PC) schemes are classified to five types: (1) Deadbeat PC, (2) hysteresis-based PC, (3) trajectory-based PC, (4) model PC (MPC), and (5) many other PC techniques which vary in optimal decision-making criterias [27]. The deadbeat predictive technique utilizes the system model to determine the appropriate control variable, which will cancel the error between the reference value and actual value of the control variables [28,29]. By the help of space-vector modulation (SVM), the switching signals are applied to the converter. The deadbeat PC produces an excellent dynamic response, however, the performance obtained from the system degrades following variations and disturbances. Furthermore, it is difficult to integrate the non-linearities and the constraints of the system [28,29]. Predictive control strategies focused on hysteresis and trajectory do not involve a modulation block and explicitly add the switching states to the converter [27,28].

Currently, the MPC is known as an easy and effective control technique for the operation of power converters and electric motors, thanks to its advantages such as simple implementation in multivariate systems, recognition of non-linearities/constraints, and excellent dynamics. The model predictive control employs a mathematical model for predicting the behavior of the system, then minimize the predefined cost function to accomplish the required control objectives [30]. The MPC schemes can be divided into two main groups: Continuous control set MPC (CCS-MPC) and finite-control-set model predictive control (FCS-MPC). The advantages of CCS-MPC is its ability for easily including of non linearities/constraints and the switching frequency is constant [31]. However, it is not possible to implement the whole control system online using a simple hardware platform. In the FCS-MPC, the question of computational optimization time is minimized by the use of the limited number of switching states. Therefore, the FCS-MPC can be implemented easily employing simple hardware [32–34].

The FCS-MPC offer high performance, quick response, and ability to handle multiple variables and constraints to achieve an optimized behavior of the system [35–38]. In spite

of the power of the FCS-MPC, it also has some drawbacks that make its utilization in drive systems very complicated [39]. The FCS-MPC is characterized by the application of only one voltage vector (VV) during one control period, which produces a high steady state ripple [40–42]. The solution to achieve a high steady state control performance in FCS-MPC is using a high sampling frequency. However, this solution entails a high computational burden [43] and an expensive digital signal processor (DSP) or FPGA (Field Programmable Gates Array) hardware. Therefore, improving the steady state performance without rising the sampling frequency of FCS-MPC algorithm is necessary and desirable. Finally, FCS-MPC takes the discrete nature of the converter into consideration. As a result, FCS-MPC does not use the entire converter control area, just the real states of the converter (Figure 1). For this purpose, with this possibility, the cost function can choose several times the same discrete real state as the optimal state, which implies that the FCS-MPC has a non-constant switching frequency [44].

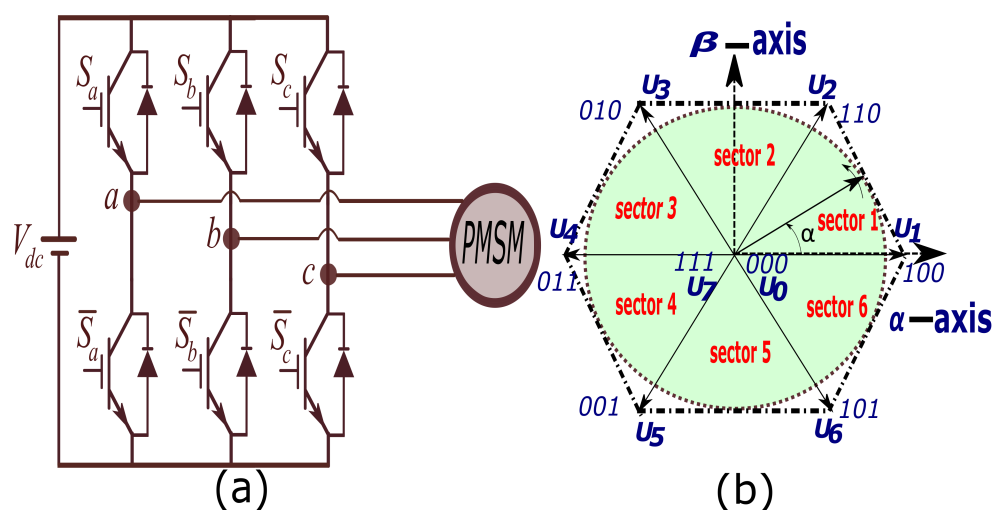


Figure 1. PMSM drive system: (a) Two-Level voltage source inverter. (b) Voltage vectors.

To solve the problem due to the uncertainty of the selection of the voltage vector (VV) and the variable switching frequency in the conventional FCS-MPC, a considerable amount of research has been proposed in this context. As in [39], the author proposed a FCS-MPC applied to a PMSM where he combined two voltage vectors (VV) based on the optimization of the duty cycle. For example if a vector is selected, there will be three other candidates of the second vector, which leads to 18 combinations to be calculated (18 iterations). Another scheme studying the use of two voltage vectors in a single control period was proposed by [45], where a universal multiple-vector-based MPC (UMV-MPC) was applied on an induction motor. The optimal voltage vector and its corresponding duty ratio is calculated directly by deadbeat control based on space-vector modulation (SVM). However, the introduction of duty cycle control in FCS-MPC increases the complexity of the control. The cost function is evaluating by only three vectors, considering the sign of torque or flux deviation in [46]. The author in [47] preselected just a part of available voltage vectors and the others are prohibited in the prediction process. In [48], a generalized multiple-vector-based model predictive control for PMSM drives is proposed. The proposed method demonstrates good steady state performance, however the control complexity is relatively high. To reduce the computational load, the deadbeat principles are integrated with the conventional FCS-MPC in [49]. However, only one voltage vector is applied in the whole sample, i.e., poor steady-state response.

In [44], a method was proposed based on FCS-MPC using a discrete space vector modulation (DSVM) with virtual switching vectors, the author takes into consideration the complete region of control of the converter unlike FCS-MPC, which just takes the real voltage vector states. The idea is to add virtual vectors to real discrete vectors using the concept of DSVM, and this technique presents good dynamic, but the computation

time is high due to the high number of virtual vectors (up to 4922 virtual vector), which requires powerful computing equipment, in addition an external modulator utilized to produce the switching signals. A multiple-vector direct-MPC for electrical machines and grid tied power converters with a reduced calculation burden was proposed in [50–53]. The reference voltage is calculated by a deadbeat function from the reference current in order to reduce the computational burden. Then, according to the location of this VV, real voltage vectors are employed with new virtual voltage vectors to improve the performance of the proposed controller. However, a PI controller is employed in the outer loop. Accordingly, the dynamic performance of the system is slow due to the limited bandwidth of the outer loop.

In this paper, a new multiple-vector model predictive control with fuzzy logic for PMSM drive systems has been proposed. This new technique is based on discrete space vector modulation (DSVM) employed together with conventional FCS-MPC in order to use the complete control region of the converter. The idea of this control strategy is to use the converter discrete real states with other vectors of the control region, called virtual vectors. In order to reduce the calculation burden, the reference voltage vector is computed directly from the reference current. Then, according to the selection of the sector the candidates of voltage vectors (real and virtual) are drastically diminished and the best selecting voltage vector via a cost function is applied to forming switching sequences for the next sampling period. Moreover, a fuzzy logic controller is used in the speed loop to control the rotor speed and to improve the robustness of the control strategy. The performance of the proposed method has been proved via simulation results for all operation conditions.

The remainder of this article is arranged according to the following: Section 2 reviews the mathematical modeling of PMSM. Section 3 shows the conventional FCS-MPC. Section 4 is dedicated to multiple vector FCS-MPC. In Section 5, the principle of fuzzy logic speed control is presented. The simulation results is illustrated in Section 6. Finally, Section 7 present the conclusion.

2. Drive Model

The proposed multiple vector finite-set MPC technique is implemented for a PMSM driven by a power electronics circuit, i.e., two level voltage-source-inverter (2L-VSI). In this part, the mathematical models of the PMSM and 2L-VSI are described. Figure 1a illustrates a description of the drive system topology under consideration. The dynamic equations of the stator currents, electromagnetic torque and speed in the rotating dq reference frame are expressed as follows [54]:

$$\left. \begin{aligned} \frac{d}{dt} i_d &= -\frac{R_s}{L_d} i_d + \frac{L_q}{L_d} \omega_r i_q + \frac{u_d}{L_d} \\ \frac{d}{dt} i_q &= -\frac{R_s}{L_q} i_q + \frac{L_d}{L_q} \omega_r i_d + \frac{u_q}{L_q} - \frac{\psi_p}{L_q} \omega_r \\ T_e &= \frac{3}{2} n_p \psi_p i_q \\ \frac{d}{dt} \omega_m &= \frac{T_e}{\Theta} - \frac{T_m}{\Theta} - v \omega_m \end{aligned} \right\} \quad (1)$$

where u_d , u_q , i_d , and i_q , are stator voltages [in V], and stator currents [in A], in the dq reference frame, respectively. R_s is the stator resistance [in Ω]. L_d and L_q is the direct and quadrature axis inductance respectively [in H], and we could assume $L_d \approx L_q$ (for surface mounted PMSM). $\omega_r = n_p \omega_m$ is the rotor electrical speed [in rad/s] (n_p is the pole-pair number and ω_m is the rotor mechanical speed). T_e [in N m] is the electromagnetic torque and T_m is the mechanical load torque applied. Θ and v are the rotor inertia [in kg/m²] and the viscous friction coefficient [in N m s], respectively.

3. Traditional Finite-Control-Set Model Predictive Control (FCS-MPC)

In this work, a common used three phase source inverter is coupled to the permanent magnet synchronous motor as shown in Figure 1a. This inverter has eight different

switching vectors and, accordingly, eight voltage vectors $u_0 - u_7$ are produced. There are six nonzero vectors and two zero vectors. Figure 1b and Table 1 show the amplitude of the active voltage vectors in the stationary reference frame $\alpha\beta$. To design the traditional FCS-MPC a discrete time model is required to predict the currents at the future sample period. Therefore, the forward Euler method is applied to the time continuous model (1) with a sampling time period T_s [in s]. For small $T_s \ll 1$, the following holds $x(k) := x(kT_s) \approx x(t)$ and $\frac{d}{dt}x(t) = \frac{x(k+1)-x(k)}{T_s}$ for all $t \in [kT_s, (k+1)T_s]$ and $k \in \mathbb{N} \cup \{0\}$. Hence, the discrete-time of the PMSM in the rotating dq -reference frame can be expressed as follows [23]:

$$\left. \begin{aligned} i_d(k+1) &= \left(1 - \frac{R_s T_s}{L_d}\right) i_d(k) + T_s \omega_r(k) i_q(k) + \frac{T_s}{L_d} u_d(k) \\ i_q(k+1) &= \left(1 - \frac{R_s T_s}{L_q}\right) i_q(k) - T_s \omega_r(k) i_d(k) + \frac{T_s}{L_q} u_q(k) - \frac{T_s \psi_p}{L_q} \omega_r(k) \end{aligned} \right\} \quad (2)$$

The stator voltage u_{dq} of the PMSM can be represented as a function of the switching vector $s^{abc}[k] \in \{0, 1\}^3$ of the inverter as follows [24]:

$$u_{dq}(k) = \left. \begin{aligned} &\underbrace{\begin{bmatrix} \cos \phi_r & \sin \phi_r \\ -\sin \phi_r & \cos \phi_r \end{bmatrix}}_{=:T_P(\phi_r)^{-1}} \underbrace{\frac{2}{3} \begin{bmatrix} 1 & -\frac{1}{2} & -\frac{1}{2} \\ 0 & \frac{\sqrt{3}}{2} & -\frac{\sqrt{3}}{2} \end{bmatrix}}_{=:T_C} \\ &\frac{1}{3} u_{dc}[k] \underbrace{\begin{bmatrix} 2 & -1 & -1 \\ -1 & 2 & -1 \\ -1 & -1 & 2 \end{bmatrix}}_{=:u_{abc}} s_{abc}[k] \end{aligned} \right\} \quad (3)$$

where, $T_P(\phi_r)^{-1}$ and T_C are inverse Park and Clarke transformations, respectively. u_{dc} is the DC-Bus voltage [in V] and u_{abc} is the stator voltage in the abc frame [in V]. $\phi_r = n_p \phi_m$ is the electrical rotor position of the PMSM [in rad]. $s_{abc} = (s_a, s_b, s_c)^T$ represent the switching states of each leg of the voltage source inverter as shown in Table 1.

Table 1. Different switching modes and corresponding voltage vector of the voltage source converter.

Conducting Modes	Switching States			Output Voltage	
	S_a	S_b	S_c	U_α	U_β
U_0	0	0	0	0	0
U_1	1	0	0	$\frac{2V_{dc}}{3}$	0
U_2	1	1	0	$\frac{V_{dc}}{3}$	$\frac{\sqrt{3}V_{dc}}{3}$
U_3	0	1	0	$-\frac{V_{dc}}{3}$	$\frac{\sqrt{3}V_{dc}}{3}$
U_4	0	1	1	$\frac{2V_{dc}}{3}$	0
U_5	0	0	1	$-\frac{V_{dc}}{3}$	$-\frac{\sqrt{3}V_{dc}}{3}$
U_6	1	0	1	$\frac{V_{dc}}{3}$	$-\frac{\sqrt{3}V_{dc}}{3}$
U_7	1	1	1	0	0

Figure 2 shows the control scheme of the traditional finite-set-control MPC, seven vectors are predicted by the discrete-time predictive model according to (2). Then, the seven predicted vectors are evaluated during the whole sampling period in order to choose the states that minimizes the cost function and achieve the minimum absolute error between the predictive current ($i_d[k+1], i_q[k+1]$) and the reference ones [42]. The cost function formula is defined as:

$$g = |i_{d,ref}[k+1] - i_d[k+1]_{u_0, \dots, 7}| + |i_{q,ref}[k+1] - i_q[k+1]_{u_0, \dots, 7}| + \begin{cases} 0 & \text{if } \sqrt{i_d[k+1]^2 + i_q[k+1]^2} \leq i_{max} \\ \infty & \text{if } \sqrt{i_d[k+1]^2 + i_q[k+1]^2} > i_{max} \end{cases} \quad (4)$$

where, the first part indicates the reduction of the reactive power, the second part is for the tracking of the torque producing current, and the last part is for the maximum allowable stator current of the PMSM. i_{max} is the maximum current allowed for the direct and quadrature axis d and q , respectively. $i_{d,ref}[k + 1]$ and $i_{q,ref}[k + 1]$ are the future reference currents predicted from the previous sampling instants $[k], [k - 1]$, and $[k - 2]$ using Lagrange extrapolation as [27]:

$$i_{dq,ref}[k + 1] = 3i_{dq,ref}[k] - 3i_{dq,ref}[k - 1] + i_{dq,ref}[k - 2]. \tag{5}$$

The main drawbacks of the traditional FCS-MPC technique are: (1) High computational load, (2) high steady state ripple due to using only one voltage vector during one control period, and (3) an expensive compute platform. These disadvantages have a negative impact on the drive system (electric motor, inverter, transmission, etc.).

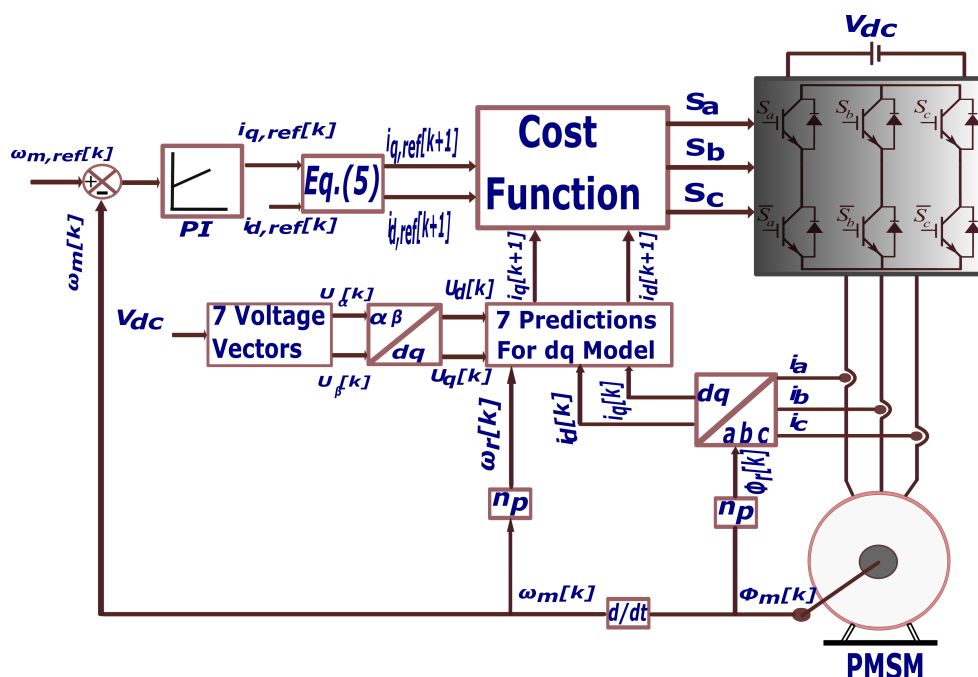


Figure 2. Conventional FCS-MPC (finite-control-set model predictive control) for a permanent-magnet synchronous motor (PMSM) drive system.

4. Proposed Multiple-Vector FCS-MPC

Following the drawbacks of traditional FCS-MPC, a discrete space vector modulation (DSVM) is employed to avoid these disadvantages. The concept of DSVM was implemented to reduce the ripples in the waveforms of the torque and current [55].

The major concept of using DSVM in FCS-MPC is for using additional virtual voltage vectors (VVs) besides the real VVs in order to scan the entire control region of the converter. In Figure 3a, the converter has three discrete real states (rounds marks) and three additional virtual VVs (square marks) in each sector. Then, two VVs will be applied for each sample instead of one VV, i.e., the switching period will be divided into two parts, for example “00” voltage vector (VV) will be applied in the first part of the period and “11” in the second part, and to achieve better results, three voltage vectors will be applied per period (3 VVs) as shown in Figure 3b. The determination of these virtual vectors V_{vir} is given by this linear combination of the real vectors, where each real vector is applied with a quantity at a given time in a commutation sequence V_{real} [44]:

$$V_{vir} = \sum_{j=1,2,3} t_j V_{real}^j \tag{6}$$

$$V_{real}^j \in \{u_0, \dots, 7\}.$$

The schematic diagram of the proposed multiple-vector FCS-MPC technique is illustrated in Figure 4. In order to reduce computational burden, the reference voltage vectors (VV) $(u_{d,ref}(k), u_{q,ref}(k))$ are computed directly by replacing $i_{dq}(k + 1)$ with $i_{dq,ref}(k + 1)$ in (2):

$$\left. \begin{aligned} u_{d,ref}(k) &= R_s i_d(k) + L_d \frac{i_{d,ref}(k+1) - i_d(k)}{T_s} - \omega_r(k) L_d i_q(k) \\ u_{q,ref}(k) &= R_s i_q(k) + L_q \frac{i_{q,ref}(k+1) - i_q(k)}{T_s} + \omega_r(k) [L_q i_d(k) + \psi_p]. \end{aligned} \right\} \quad (7)$$

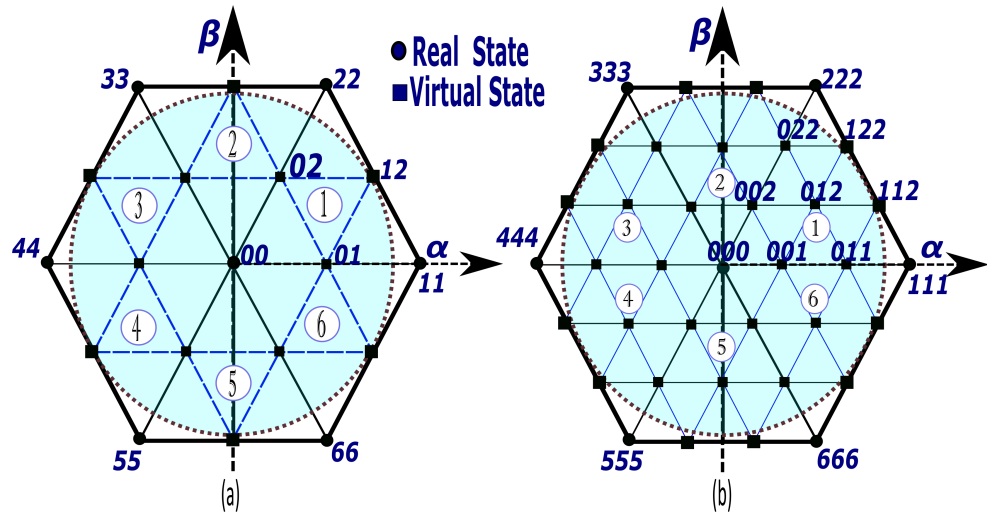


Figure 3. Control region of the two level voltage-source-inverter (2L-VSI) in $\alpha\beta$ reference frame with: (a) Three additional virtual voltage vectors (VVs)/sector, and (b) seven additional virtual voltage vectors /sector.

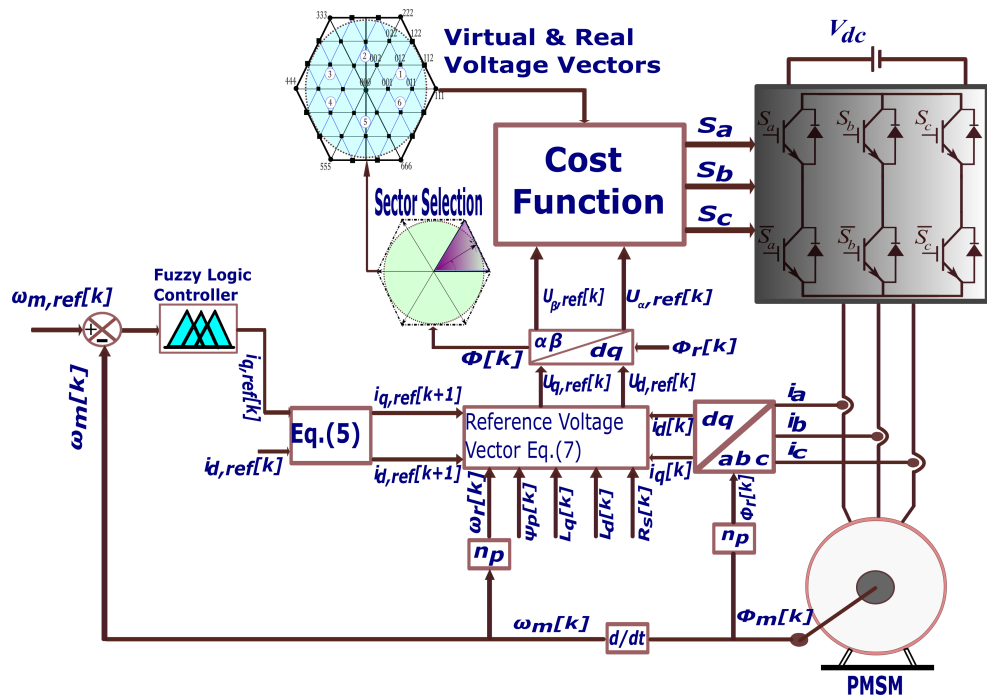


Figure 4. Proposed FCS-MPC with multiple-vector for PMSM drive system.

Then, using Park transformation, this reference voltage computed in (7) $u_{dq,ref}(k)$ based on the rotating frame is converted into the $\alpha\beta$ stationary reference frame $(u_{\alpha,ref}(k), u_{\beta,ref}(k))^T$. The location of this voltage is determined by its angle as illustrated in Figure 3b.

$$\phi(k) = \text{atan2}(u_{\beta,ref}(k), u_{\alpha,ref}(k)) \quad (8)$$

According to this angle, only one sector is selected. Consequently, the cost function turns into this form:

$$g = |u_{\alpha,ref}(k) - u_{\alpha}(k)| + |u_{\beta,ref}(k) - u_{\beta}(k)|. \quad (9)$$

The quality function (9) is iterated 6 and 10 times, respectively, for (2VV)-MV-FCS-MPC and (3VV)-FCS-MPC, which implies that the computational burden of the suggested MV-FCS-MPC is smaller than that of the system proposed in [44].

The algorithm of the proposed MV-FCS-MPC with the improvement of the steady state performance is given by the flow chart in Figure 5, where N_{VV} is the number of voltage vectors (real and virtual VVs) for each sector.

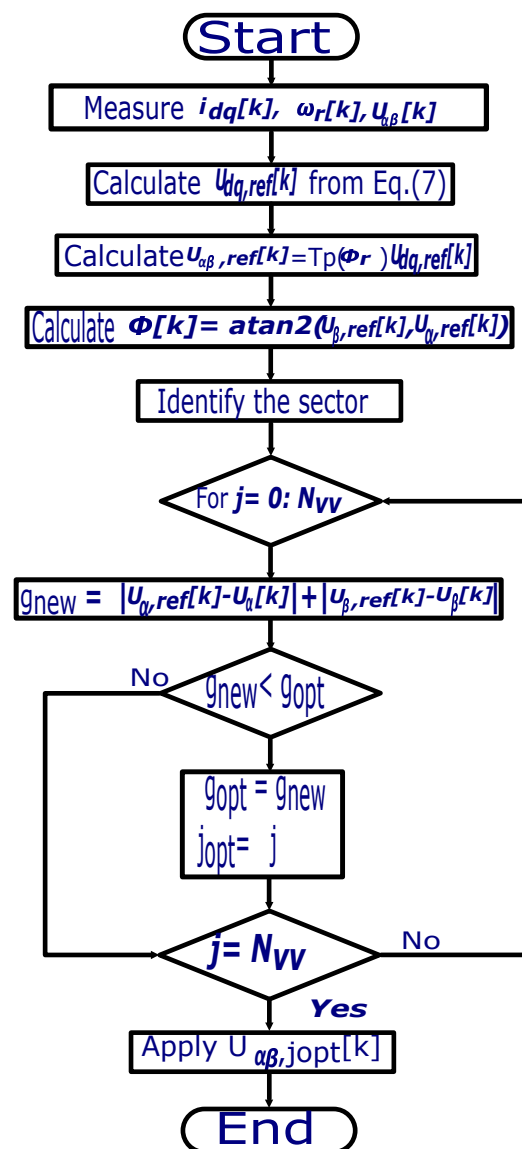


Figure 5. Flowchart of the Proposed Finite-Control-Set Model Predictive Control with Multiple-vector.

5. Fuzzy Logic Speed Control

Conventional PI type controllers are widely used. They are subject to deterioration in performance in the presence of load disturbances and parametric variations. To compensate for these degradation, the use of modern and intelligent controls is more than necessary [54]. A number of these commands have already been applied to the PMSM such as fuzzy control, adaptive control, and neural networks. In our work fuzzy logic constitutes an interesting alternative considering several advantages such as: Reasoning close to the natural reasoning of the operator, independence from modeling, the capacity to control a non linear system, frequent enhancement of dynamic performance, and its intrinsic qualities of robustness (i.e., no dependency of the parameters of the system under control). In fuzzy logic control, the linguistic description of human expertise is represented in the form of fuzzy rules in order to control the system [56].

5.1. Architecture of Fuzzy Logic Control System

A fuzzy system is formed of three steps as shown in Figure 6. First, the fuzzification step transforms the numerical values into degrees of belonging to the different fuzzy sets of the partition [56,57]. The second step concerns the inference module, which consists of two blocks, the inference engine and the base of the rules. Finally, the defuzzification step allows to infer a (precise) net value, usable in command for example, from the result of the aggregation of the rules [56,57].

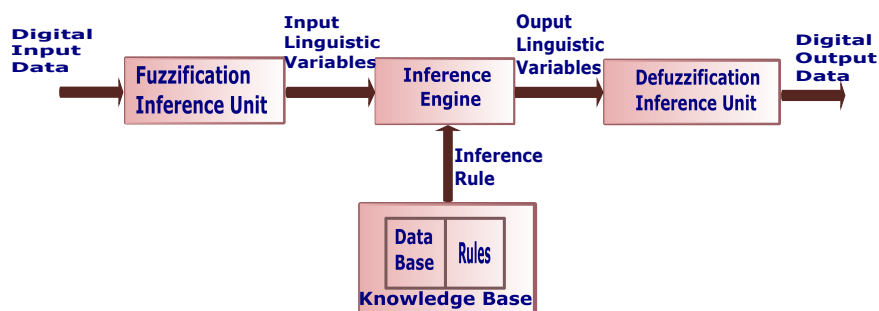


Figure 6. Block diagram of the fuzzy system.

5.2. Fuzzy Logic Controller

The PI speed controller in the traditional FCS-MPC method is replaced by a fuzzy controller in the proposed method MV-FCS-MPC presented in Figure 7. In the case of a fuzzy speed control, the error is usually needed, e , and the error derivative, de . The output signal is determined according to the input signals via the fuzzy rules [56–58].

$$e = \omega_{ref}(k) - \omega_m(k) \tag{10}$$

$$de = e(k) - e(k - 1) \tag{11}$$

where ω_{ref} is the desired speed and $\omega_m(k)$ is the measured or actual speed.

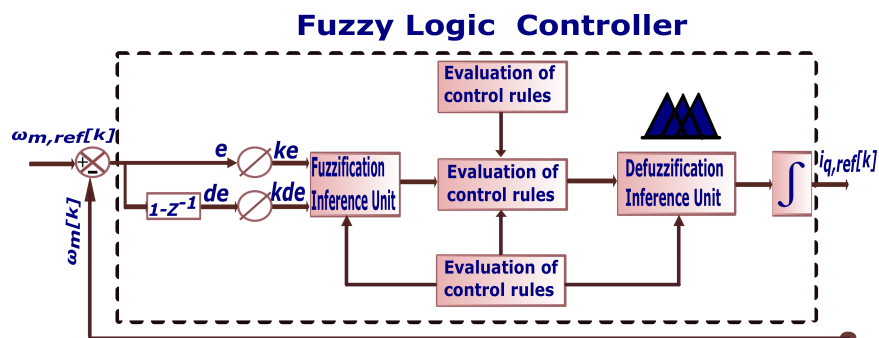


Figure 7. Fuzzy logic controller.

The fuzzy inference (fuzzification) is done employing Memdani's method [59–61], and the defuzzification is realized by using the center of gravity method to calculate this controller's output. The control rules that required to change the numerical variables into linguistic ones are indicated in Table 2, where the abbreviations in this table is defined as follows: Negative big (NB), negative medium (NM), negative small (NS), zero (ZE), positive small (PS), positive medium (PM), and positive big (PB) [59–61].

Table 2. Rule base for speed control. Negative big (NB), negative medium (NM), negative small (NS), zero (ZE), positive small (PS), positive medium (PM), and positive big (PB).

$e \backslash de$	NB	NM	NS	ZE	PS	PM	PB
NB	NS	NS	NS	NB	NM	NS	ZE
NM	NS	NS	NB	NM	NS	ZE	PS
NS	NS	NB	NM	NS	ZE	PS	PM
ZE	NB	NM	NS	ZE	PS	PM	PB
PS	NM	NS	ZE	PS	PM	PB	PS
PM	NS	ZE	PS	PM	PB	PS	PB
PB	ZE	PS	PM	PB	PS	PB	PB

Based on Table 2, $7 \times 7 = 49$ rules are defined based on the signals e and de . In order to declare the working principles of this fuzzy controller, the following rules are described.

1. If the values of $e(k)$ and $de(k)$ are NB, the value of the output will be NS;
2. If the values of $e(k)$ and $de(k)$ are PB and NM, respectively, the value of the output will be PS;
3. If the values of $e(k)$ and $de(k)$ are ZE and NS, respectively, the value of the output will be NS;
4. If the values of $e(k)$ and $de(k)$ are NS and NB, respectively, the value of the output will be NS.

6. Simulation Results and Discussion

In this section, the proposed multiple vector FCS-MPC with fuzzy logic controller applied on a PMSM drive system is simulated using Matlab/Simulink software. The performance of a traditional FCS-MPC, two voltage vector FCS-MPC, and three voltage FCS-MPC will be discussed and compared in detail. The nominal parameters of the PMSM are defined in Table 3. The proposed multiple vector FCS-MPC method uses the model presented in Figure 4.

Table 3. PMSM drive parameters.

Variable	Symbol	Value
d axis inductance [mH]	L_d	15
q axis inductance [mH]	L_q	15
Flux induced by magnets [Wb]	ψ_p	0.85
Number of poles	n_p	3
Rotor inertia [kg/m^2]	Θ	0.002
viscous friction [N m s]	v	0.0015
Stator resistance [Ω]	R_s	0.2
Rated power [kw]	P	16
DC-link [V]	V_{dc}	560
Sampling time for all methods [μs]	T_s	40

After presenting the theory of the traditional FCS-MPC, we will analyze the behavior of the electric drive system by this technique. Figure 2 shows a diagram of the traditional FCS-MPC command, with PI parameters of $k_p = 0.28$ and $k_i = 1$ obtained based on the symmetrical optimum method, the goal is to check if our technique is implantable in real time and to observe the behavior of the system through various studied modes, which improves the performance of the electric drive system. The ability to change speed of the system with robustness is a primary concern, as the system response for this property is used extensively to verify the driving quality of the electric drive system.

Figure 8a,b show the motor speed and the tracking error. According to this figure, the speed begins from 250 rpm, then changes to 500 rpm at (0.3 s), and 750 rpm at 0.5 (s). The measured rotational speed varies depending on the reference and we see that there is good tracking dynamics at the mechanical load torque $T_m = 1$ [N m], but there is a large overshoot until 288 rpm at start-up and 526 rpm and 772 rpm when changing the speed. In addition, we note that the tracking error is almost zero during all simulation time except at the start and speed change at 0.3 s and 0.5 s. Note that, in Figure 8a, the speed is not strictly superimposed on its reference, it is slightly lower than its reference (non zero steady-state error) due to the drawbacks of the PI controller such as sensitivity to controller gains and sluggish response to sudden disturbances.

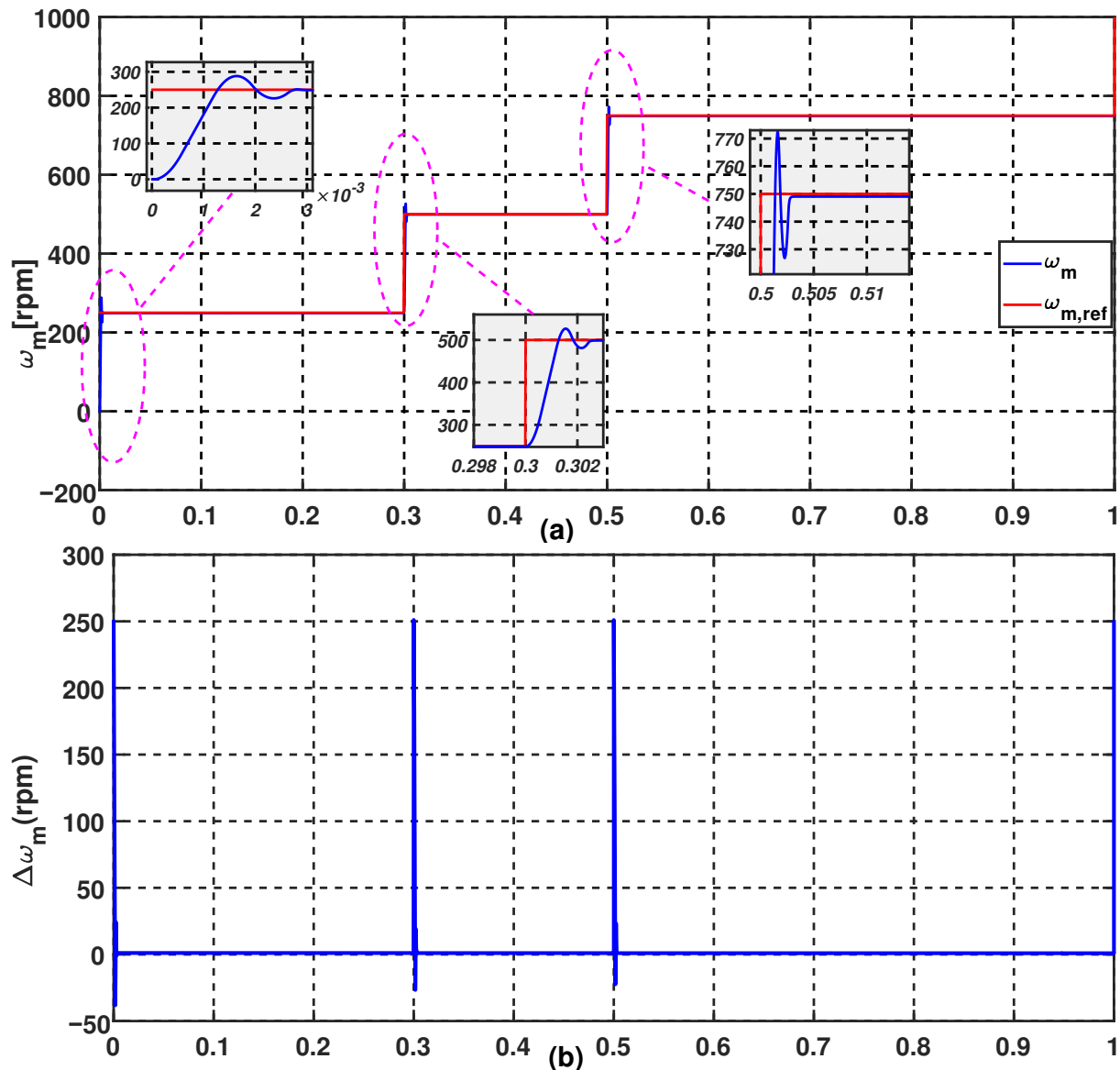


Figure 8. Cont.

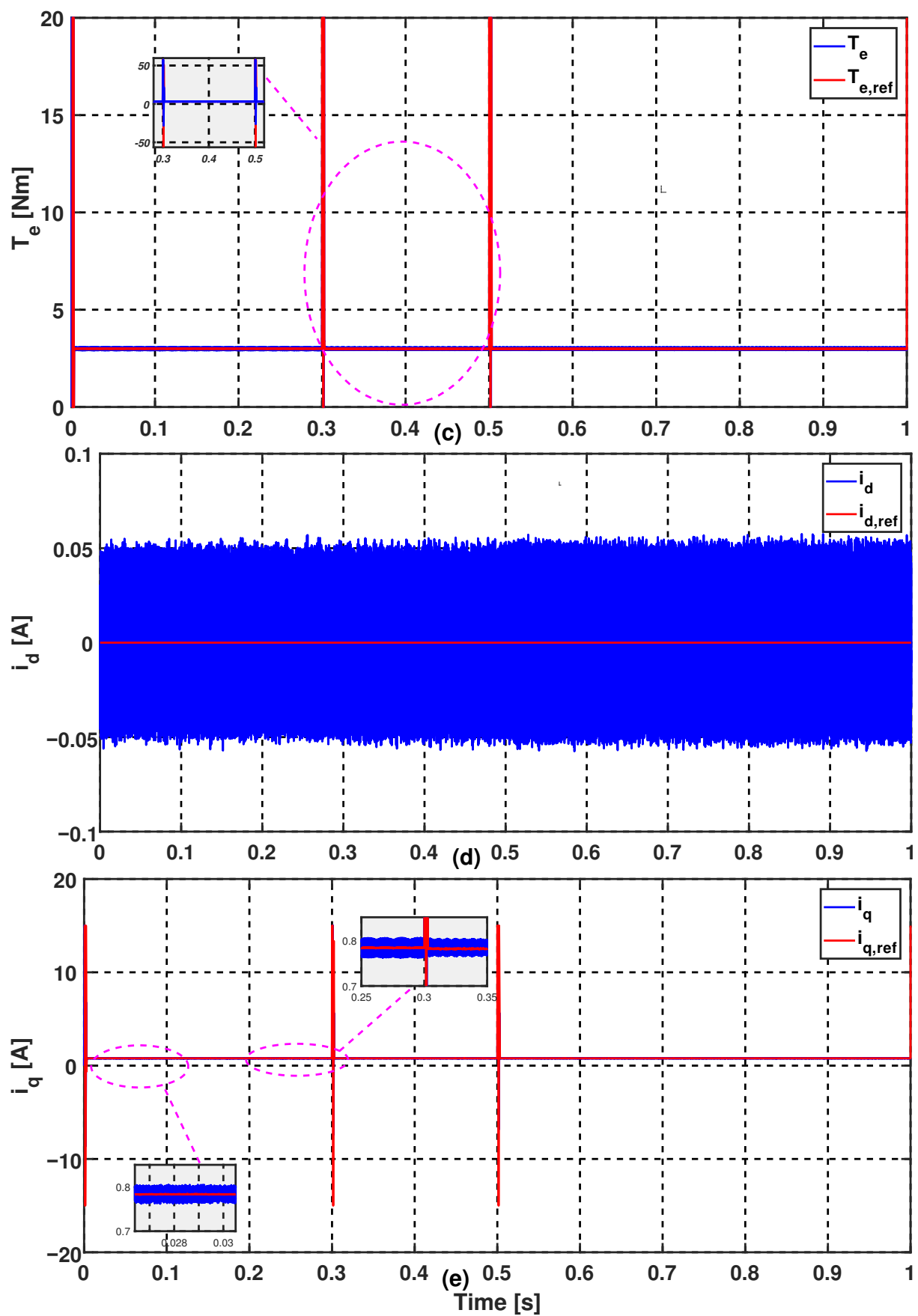


Figure 8. Performances of the traditional FCS-MPC applied on PMSM drive system (from top): (a) Speed ($\omega_m, \omega_{m,ref}$), (b) tracking error ($\Delta\omega_m$), (c) electromagnetic torque ($T_e, T_{e,ref}$), (d) direct current ($I_d, I_{d,ref}$), and (e) quadratic current ($I_q, I_{q,ref}$).

Figure 8d,e shows the results of d - and q -axis currents, as it is mentioned in the description of the control technique, it can be observed that this strategy keeps the direct current at zero force the quadratic component to react to the torque disturbance, which proves the good monitoring performance of the controller ($i_{d,ref} = 0$). The current i_q and the electromagnetic torque have the same shape which shows the decoupling to be perfectly carried out. We can also see in Figure 8c the electric motor develops more electromagnetic torque to reach the different stages of the speed reference, reaching 57 Nm between 0.3 and 0.5 s to overcome the moment of inertia. The oscillations are all the more distinguished on the response curve of the stator currents i_{dq} . The phenomenon alters the functioning of the control, even the currents absorbed by the machine. On these curves we see that the decoupling is seriously affected by the oscillations. Accordingly, it can be concluded that the steady state performance of the traditional method is not prominent.

The performances of the proposed multiple-vector (MV) FCS-MPC method (2VV and 3VV) are presented in Figures 9 and 10, the signal plots from top to bottom are: Actual speed and its reference ($\omega_m, \omega_{m,ref}$), the tracking error ($\Delta \omega_m$), electromagnetic torque T_e , and the stator currents along the two axes d and q . The dynamic performance of the proposed method (2VV, 3VV) is better compared to the traditional FCS-MPC method. It is clear that the method proposed with its two cases (2VV and 3VV) requires a settling time of (0.011 s), while the traditional method requires a higher settling time (more than 0.05 s).

Note, that in Figures 9a and 10a the speed tracks its reference quickly and without overshooting, also, the speed is strictly centrally symmetrical with its reference resulting in a zero static error. These results show a less response time of the fuzzy regulator and high accuracy without any mathematical calculations. On the other hand, with the conventional FCS-MPC method, the settling time is sacrificed in order to avoid a large overshoot at start-up and when changing the speed.

Figures 9d,e and 10d,e represent the shapes of the two current components d and q in both cases (2VV-FCS-MPC and 3VV-FCS-MPC). The two currents are regulated independently of each other, and it exhibits a different behavior depending on the control strategy used, whether in transient or permanent conditions, and more particularly the variable i_q . Concerning the conventional method, the current i_q shows a very clear ripple whereas in the case of the multiple vector strategy FCS-MPC, we observe that the phenomenon is reduced considerably. The MV-FCS-MPC method (3VV) gives a minimum value of the ripple in the current along the q axis compared to the MV-FCS-MPC (2VV) method and the conventional method. In addition, the ripple in the current along the d axis is small in the case of FCS-MPC (3VV). But in the case of FCS-MPC (2VV), the ripple is slightly smaller compared to the traditional FCS-MPC method. This is thanks to the contribution of virtual vectors, which reduce this undesirable phenomenon.

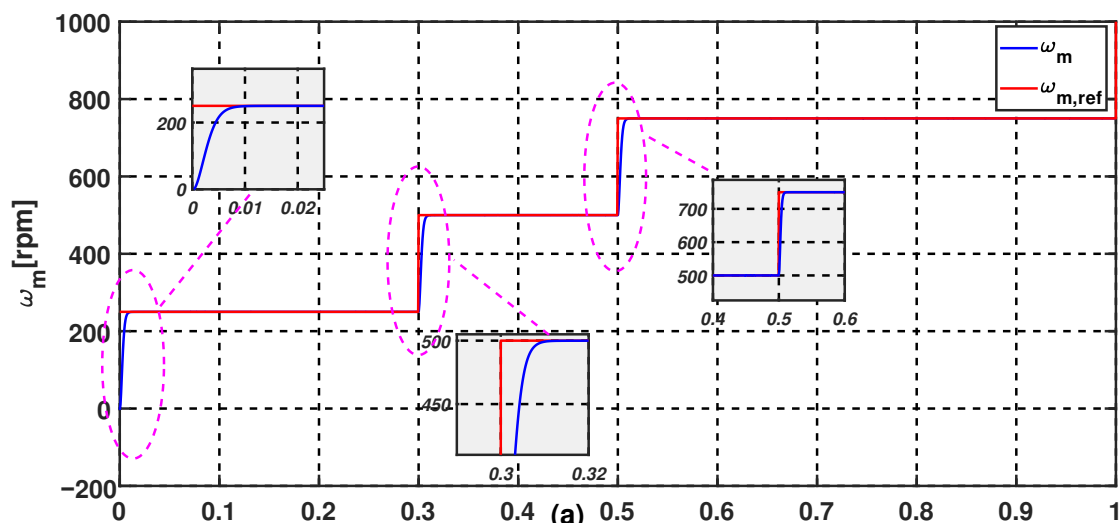


Figure 9. Cont.

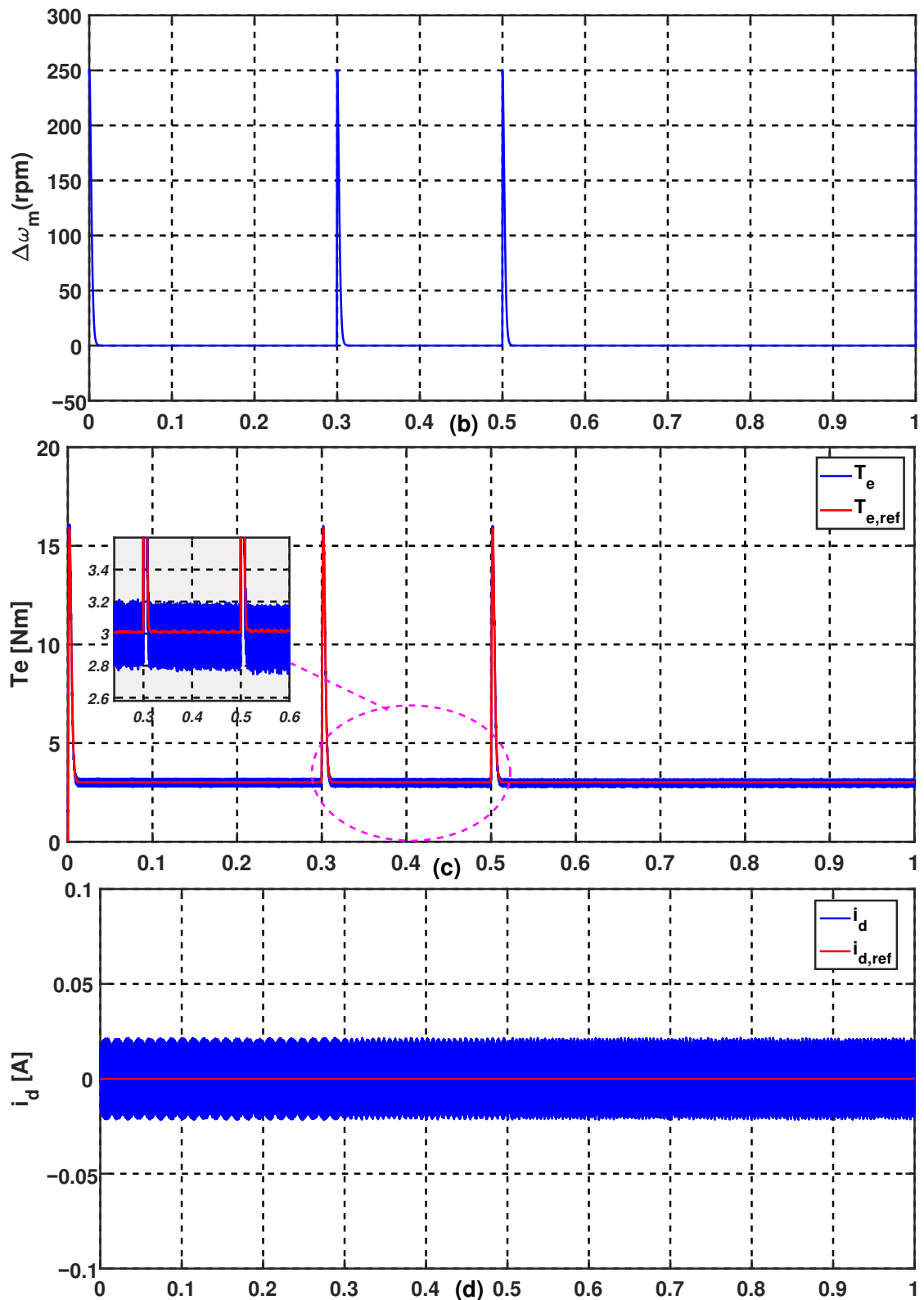


Figure 9. Cont.

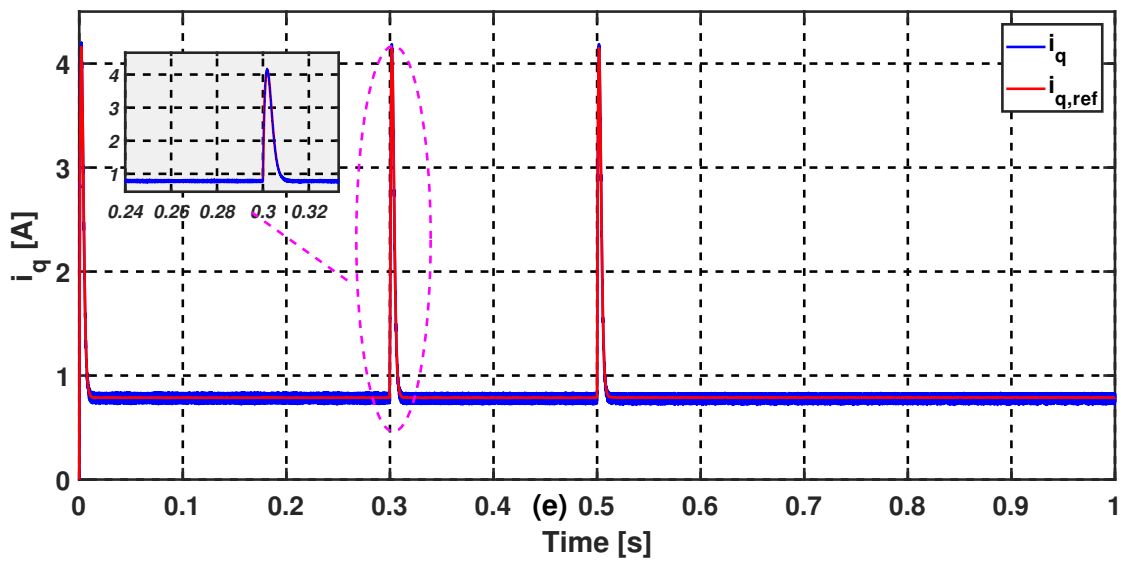


Figure 9. Performances of the proposed multiple-vector 2VV FCS-MPC applied on PMSM drive system (from top): (a) Speed ($\omega_m, \omega_{m,ref}$), (b) tracking error ($\Delta\omega_m$), (c) Eelectromagnetic torque ($T_e, T_{e,ref}$), (d) direct current ($I_d, I_{d,ref}$), and (e) quadratic current ($I_q, I_{q,ref}$).

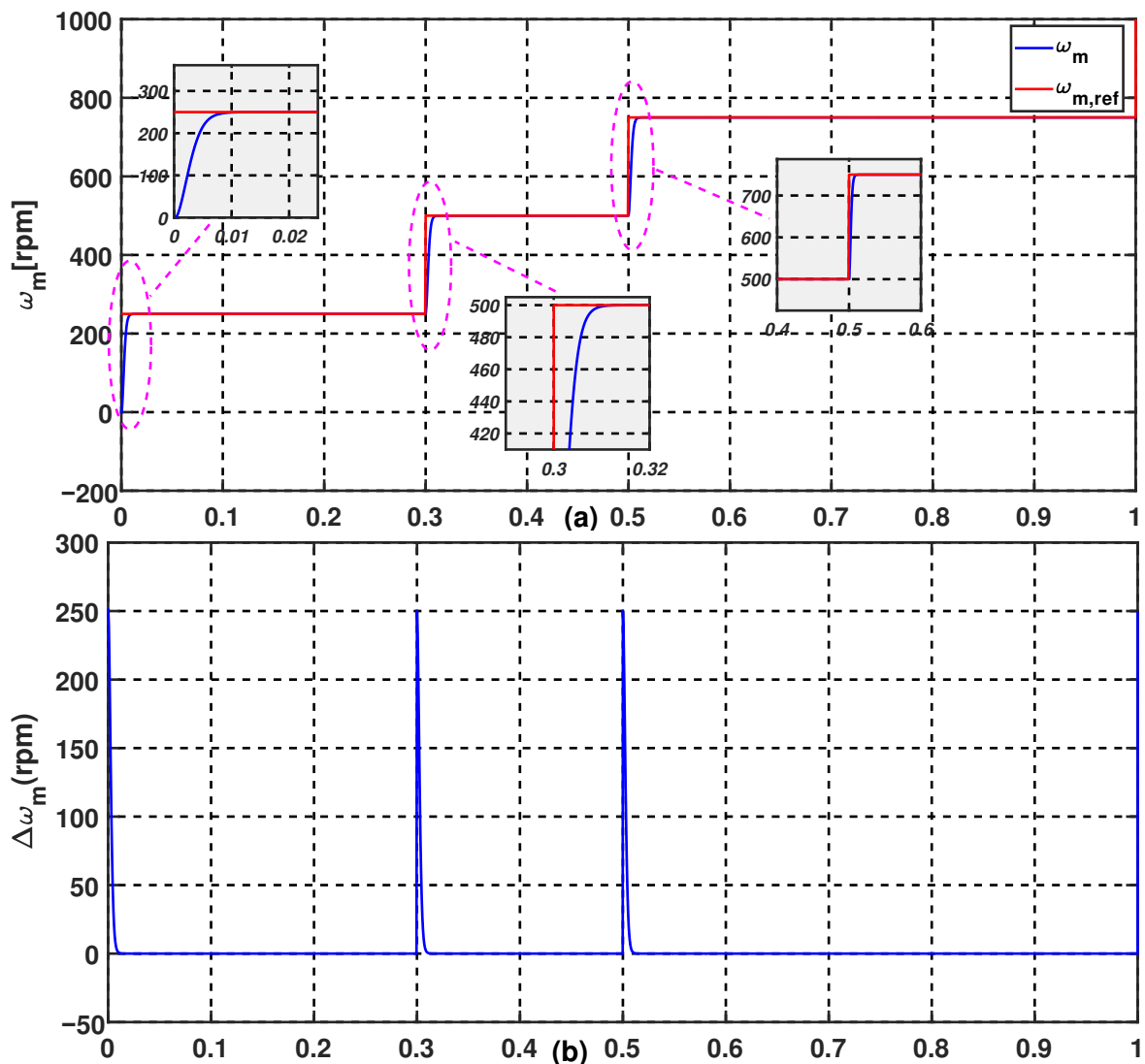


Figure 10. Cont.

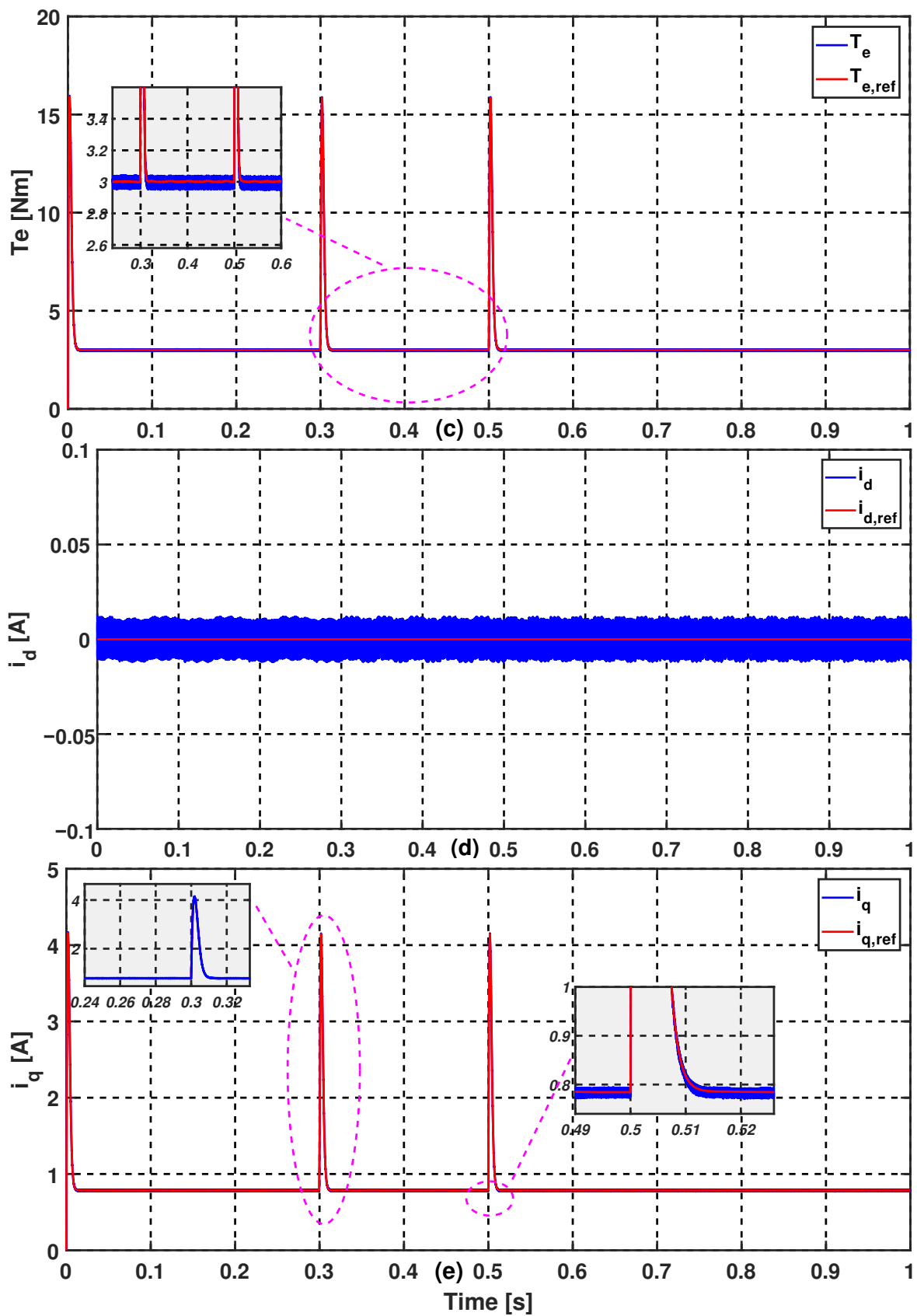


Figure 10. Performances of the proposed multiple-vector 3VV FCS-MPC applied on PMSM drive system (from top): (a) Speed ($\omega_m, \omega_{m,ref}$), (b) tracking error ($\Delta\omega_m$), (c) electromagnetic torque ($T_e, T_{e,ref}$), (d) direct current ($I_d, I_{d,ref}$), and (e) quadratic current ($I_q, I_{q,ref}$).

Figures 9c and 10c show the shape of the electromagnetic torque and its reference. As the flux is kept constant, the behavior of the electromagnetic torque remains unchanged and is almost the same as its image, the current i_q .

The wave-form of the three-phase currents for the conventional and the proposed methods are explored in Figure 11. It is clear that the waveform of the three-phase currents of the stator has a sinusoidal shape and indicates the regular operation of the PMSM motor. The amplitude of the current is proportional to the torque and changes rapidly with the load torque. Furthermore, it can be seen that the ripple of the three-phase current is lower in MV-FCS-MPC (3VV) (Figure 11c) in comparison with MV-FCS-MPC (2VV) (Figure 11b) and FCS-MPC (Figure 11a). In addition, the total harmonic distortion (THD) of the suggested method is better than the traditional one such as 1.35%, 1.88%, and 2.39% for MV-FCS-MPC (3VV), MV-FCS-MPC (2VV), and FCS-MPC respectively. The main reason is due to the use of virtual voltage vectors which give higher switching frequency and lower total harmonic distortion (THD).

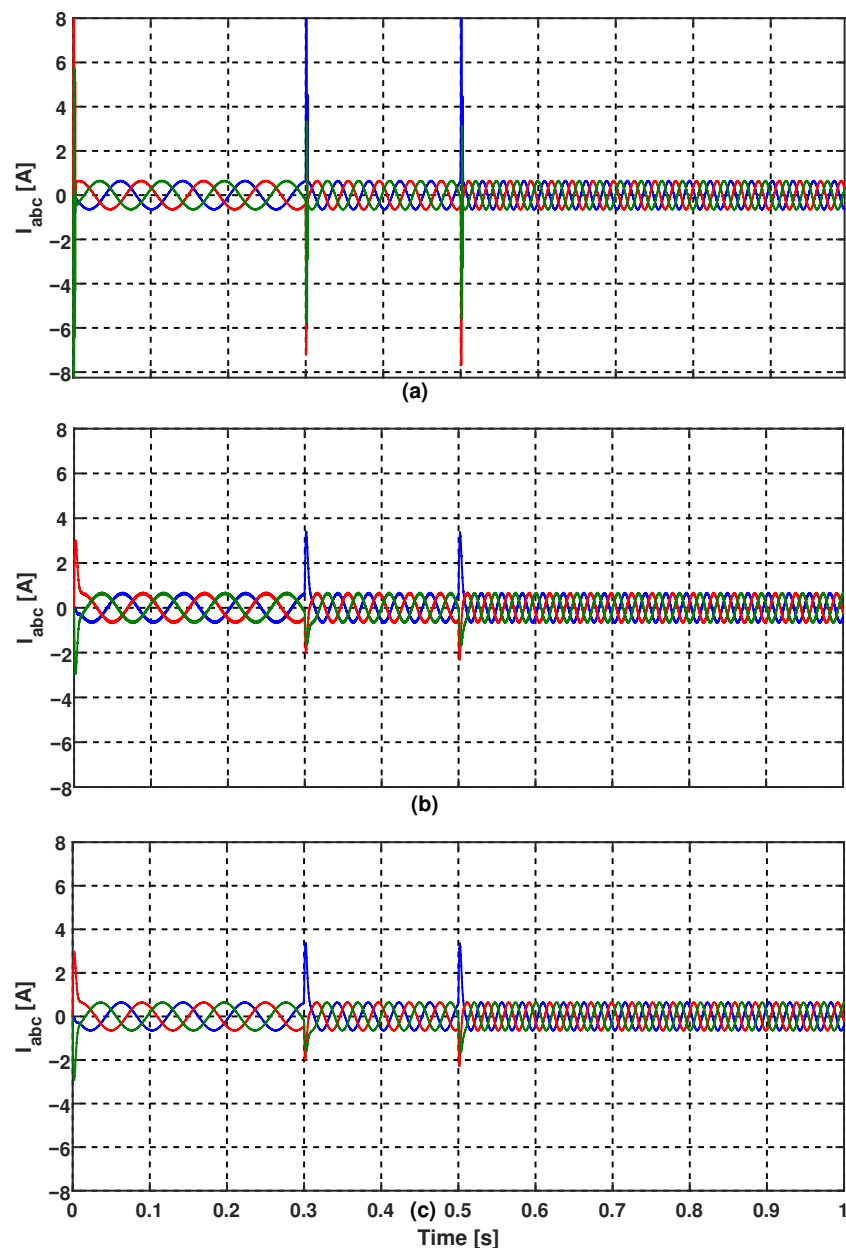


Figure 11. Three-phase currents of the PMSM in steady-state (from top): (a) Conventional FCS-MPC, (b) multiple-vector 2VV FCS-MPC, and (c) multiple-vector 3VV FCS-MPC.

In order to check the robustness of the proposed methods under (unknown) parameter variations of the PMSM, the stator resistance R_s is increased by 150% of its nominal value (e.g., due to aging or warming). For this scenario, it can be seen in Figure 12 and 13 that the proposed methods are relatively robust against parameter variation in R_s . No effects in the control performance occur due to the uncertainty in the stator resistance R_s .

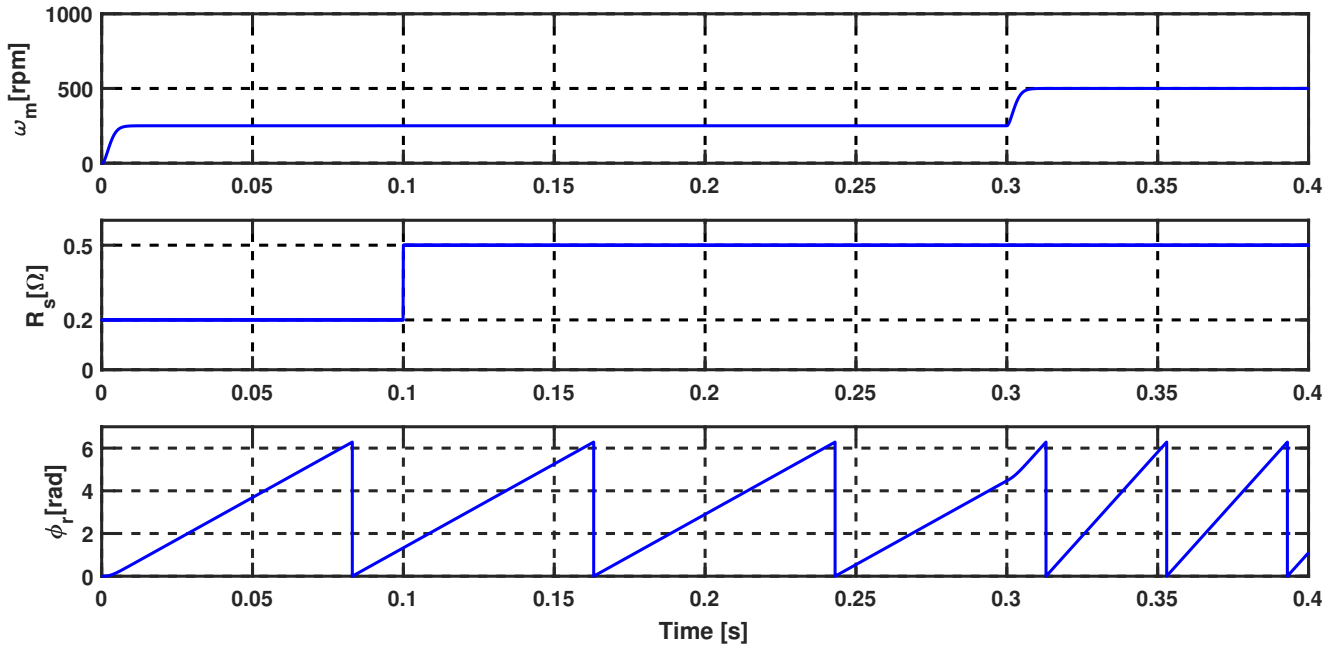


Figure 12. Simulation results of multiple vector 2VV FCS-MPC at step change in the PMSM resistance R_s (from top): Speed ω_m , resistance R_s , and rotor angle ϕ_r .

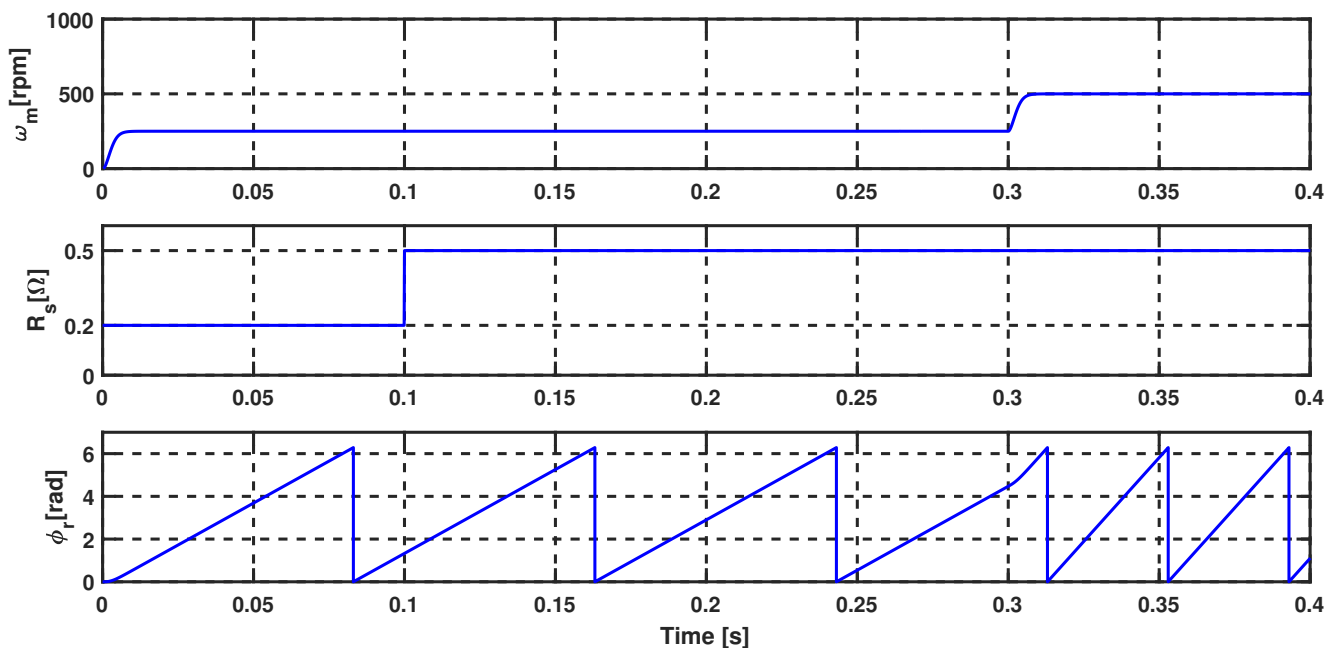


Figure 13. Simulation results of multiple vector 3VV FCS-MPC at step change in the PMSM resistance R_s (from top): Speed ω_m , resistance R_s , and rotor angle ϕ_r .

Figure 14 and 15 shows that the robustness of the proposed methods have been investigated with respect to uncertainties (due to magnetic saturation) in the stator inductance L_q of the PMSM model. Therefore, L_q is increased by 10%. Again, the proposed methods (2VV and 3VV) shows a good performance and is relatively robust against parameter uncertainties.

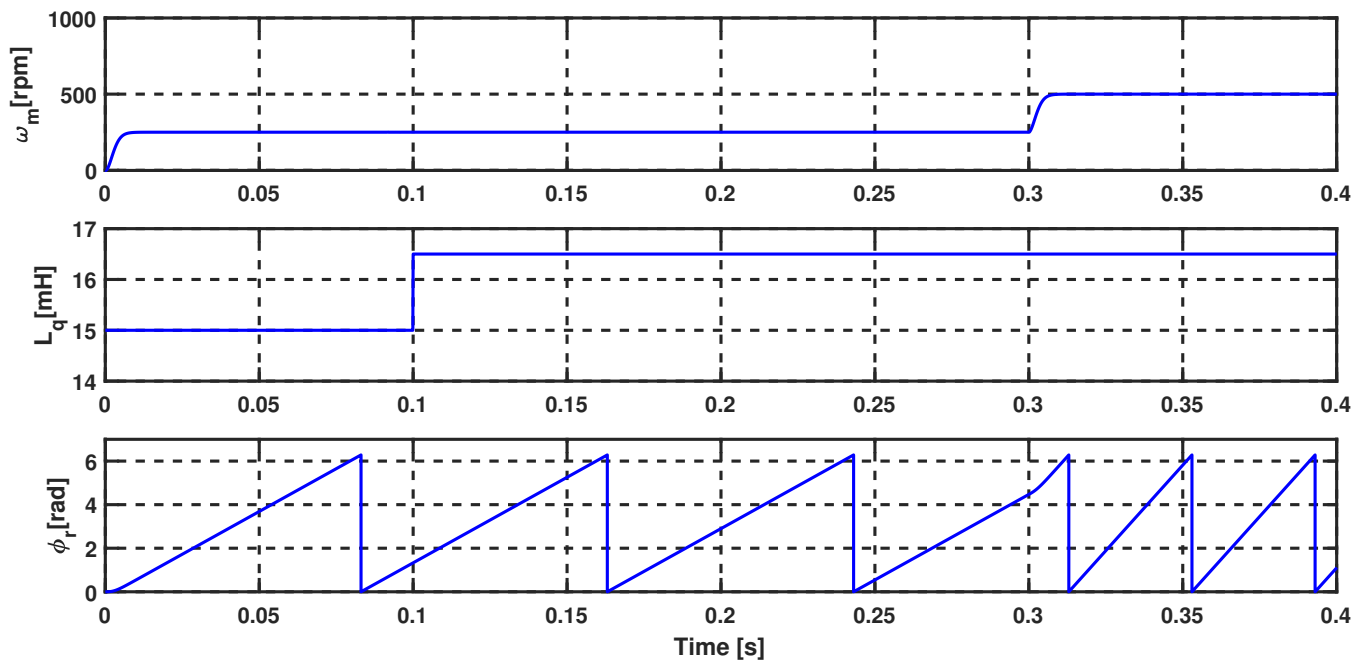


Figure 14. Simulation results of multiple vector 2VV FCS-MPC at step change in the PMSM inductance L_q (from top): Speed ω_m , inductance L_q , and rotor angle ϕ_r .

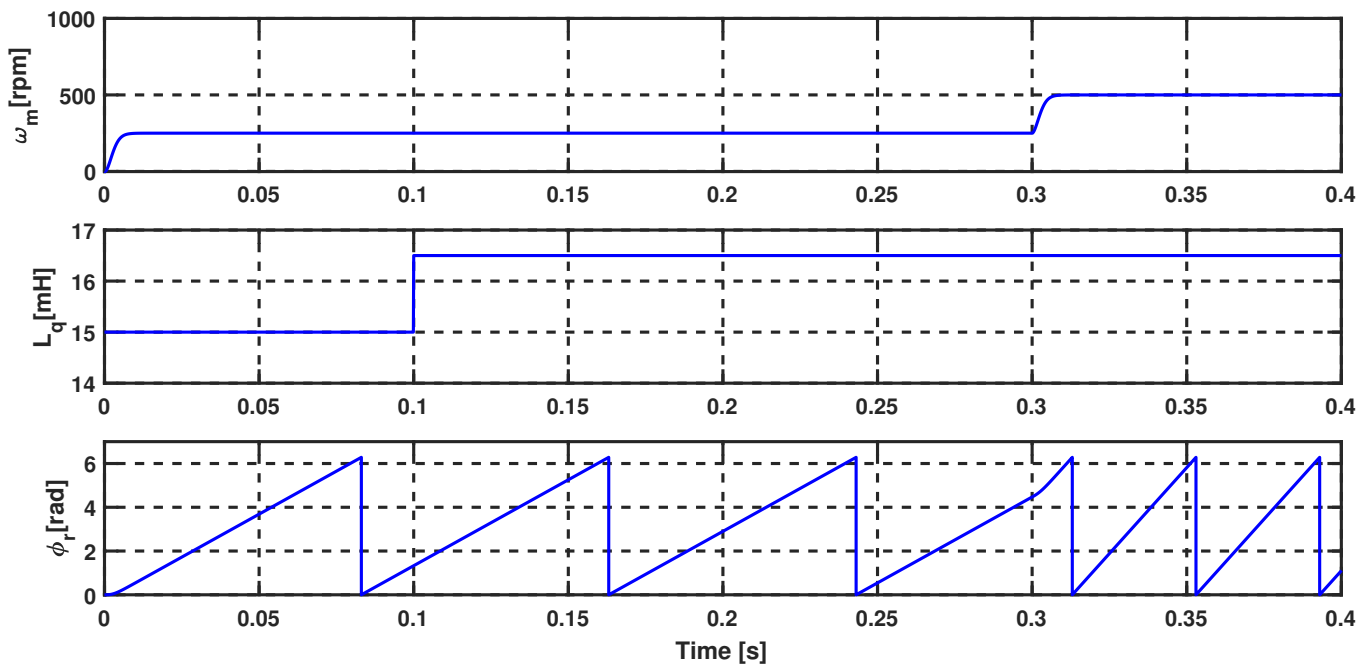


Figure 15. Simulation results of multiple vector 3VV FCS-MPC at step change in the PMSM inductance L_q (from top): Speed ω_m , inductance L_q , and rotor angle ϕ_r .

Finally, from Figure 16 the average switching frequency of the traditional FCS-MPC is 2.56 kHz while the 2VV FCS-MPC and 3VV FCS-MPC gives 3 kHz and 4 kHz respectively, which means that the switching frequency increase by adding virtual vectors. However, the THD of the currents is reduced and the steady-state performance is improved. Furthermore, it can be seen from Figure 16 that by using the proposed 2VV FCS-MPC and 3VV FCS-MPC, the change in the switching frequency (i.e., peak-peak variations) is significantly lower than in case of using the conventional FCS-MPC.

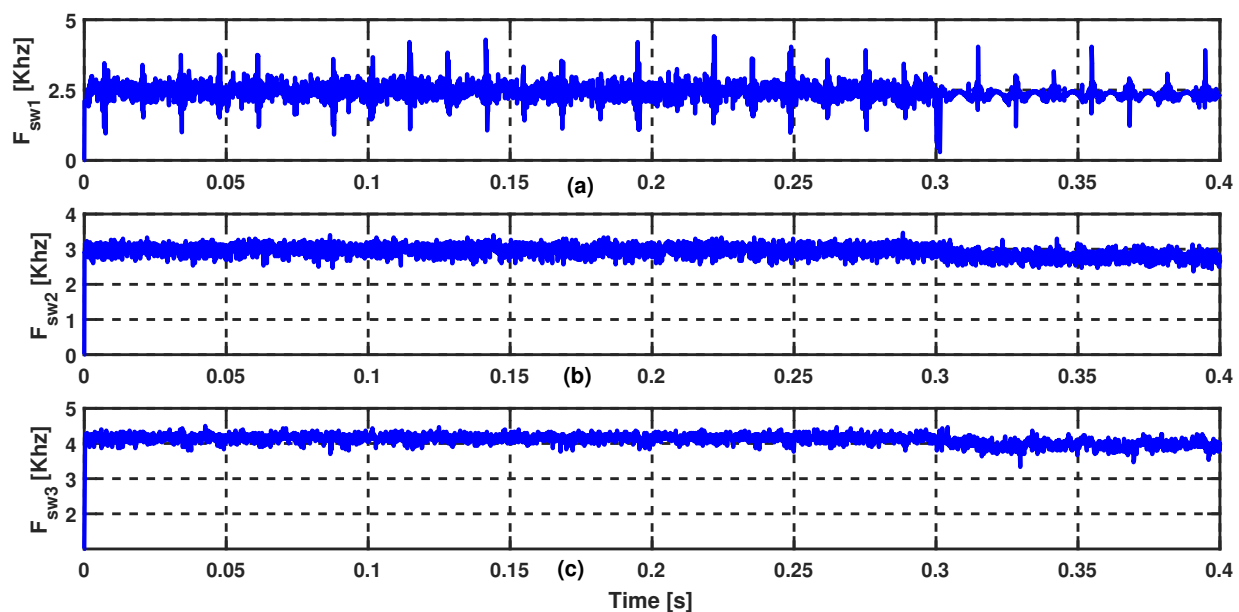


Figure 16. Switching frequency for the three methods (from top): Conventional FCS-MPC, 2VV FCS-MPC, and 3VV FCS-MPC.

7. Conclusions

There is always a large current ripple and poor steady-state performance due to the application of only one voltage vector in conventional FCS-MPC during one control time period. To overcome this problem, the present paper proposed a multiple-vector finite control set model predictive control (MV-FCS-MPC) scheme with fuzzy logic control for permanent-magnet synchronous motor (PMSM) used in an electric drive system. The proposed control technique is based on the Discrete Space Vector Modulation (DSVM), which combines the virtual voltage vectors with the real ones in order to reduce the ripples in current waveforms, therefore, improving steady state performance. Furthermore, the proposed method reduced the calculation burden by computing directly the reference voltage vector (VV) from the reference current. A simulation was conducted to validate the feasibility of the new approach and its performance was compared with the traditional FCS-MPC. The results show that the proposed method MV-FCS-MPC with 2VV and 3VV had better dynamic response than the traditional FCS-MPC. The steady state performance of MV-FCS-MPC with 3VV was better and exhibited a smaller ripple in the current waveform and lower total harmonic distortion (THD). Furthermore, the steady state performance of MV-FCS-MPC with 2VV was similar to that of FCS-MPC with the PI controller, but the dynamic response in speed was better due to the robustness of the fuzzy logic controller. Finally the experimental validation of the proposed command approach, in order to determine the validity of our simulation, is a necessary perspective in the work that follows.

Author Contributions: The developed multiple vector MPC with fuzzy logic control was suggested and designed, by I.F.B. and M.A. Furthermore, the writing of the original draft preparation was realized also by I.F.B. Writing, reviewing, and editing was done by M.A., A.T. and R.K. All authors have read and agreed to the published version of the manuscript.

Funding: For this work, no external funding was received.

Institutional Review Board Statement: Not applicable.

Informed Consent Statement: Not applicable.

Data Availability Statement: Not applicable.

Acknowledgments: This work was supported by the German Research Foundation (DFG) and the Technical University of Munich (TUM) in the framework of the Open Access Publishing Program.

Conflicts of Interest: No conflict of interest.

References

1. Deng, R.; Xiang, Y.; Huo, D.; Liu, Y.; Huang, Y.; Huang, C.; Liu, J. Exploring flexibility of electric vehicle aggregators as energy reserve. *Electr. Power Syst. Res.* **2020**, *184*, 106305. [[CrossRef](#)]
2. Wang, Y.; John, T.; Xiong, B. A two-level coordinated voltage control scheme of electric vehicle chargers in low-voltage distribution networks. *Electr. Syst. Res.* **2019**, *168*, 218–227. [[CrossRef](#)]
3. Sufyan, M.; Rahim, N.A.; Muhammad, M.A.; Tan, C.K.; Raihan, S.R.S.; Bakar, A.H.A. Charge coordination and battery lifecycle analysis of electric vehicles with v2g implementation. *Electr. Power Syst. Res.* **2020**, *184*, 106307. [[CrossRef](#)]
4. Van den Bergh, K.; Delarue, E. Energy and reserve markets: interdependency in electricity systems with a high share of renewables. *Electr. Power Syst.* **2020**, *189*, 106537. [[CrossRef](#)]
5. Salehifar, M.; Moreno-Eguilaz, M.; Putrus, G.; Barras, P. Simplified fault tolerant finite control set model predictive control of a five-phase inverter supplying bldc motor in electric vehicle drive. *Electr. Power Syst.* **2016**, *132*, 56–66. [[CrossRef](#)]
6. Rodrigues, T.; Neves, G.; Gouveia, L.; Abi-Ramia, M., Jr.; Fortes, M.; Gomes, S., Jr. Impact of electric propulsion on the electric power quality of vessels. *Electr. Power Syst. Res.* **2018**, *155*, 350–362. [[CrossRef](#)]
7. Xiao, X.; Zhang, Y.; Wang, J.; Du, H. New adaptive sliding-mode observer design for sensorless control of pmsm in electric vehicle drive system. *Int. J. Smart Sens. Intell. Syst.* **2016**, *9*, 377–396. [[CrossRef](#)]
8. Driss, S.; Farhangi, S.; Nikzad, M.R. Low switching frequency model predictive control of pmsm drives for traction applications. In Proceedings of the 2018 9th Annual Power Electronics, Drives Systems and Technologies Conference (PEDSTC), Havel, Iran, 14–15 February 2018; pp. 300–305.
9. Ayad, A.; Karamanakos, P.; Kennel, R.; Rodriguez, J. Direct model predictive control of bidirectional quasi-z-source inverters fed pmsm drives. In Proceedings of the 2017 11th IEEE International Conference on Compatibility, Power Electronics and Power Engineering (CPE-POWERENG), Cadiz, Spain, 4–6 April 2017; pp. 671–676.
10. Sun, X.; Hu, C.; Zhu, J.; Wang, S.; Zhou, W.; Yang, Z.; Lei, G.; Li, K.; Zhu, B.; Guo, Y. Mptc for pmsms of evs with multi-motor driven system considering optimal energy allocation. *IEEE Trans. Magn.* **2019**, *55*, 1–6. [[CrossRef](#)]
11. Yuan, X.; Zhang, S.; Zhang, C. Enhanced robust deadbeat predictive current control for pmsm drives. *IEEE Access* **2019**, *7*, 148218–148230. [[CrossRef](#)]
12. Buja, G.S.; Kazmierkowski, M.P. Direct torque control of pwm inverter-fed ac motors—a survey. *IEEE Trans. Ind. Electron.* **2004**, *51*, 744–757. [[CrossRef](#)]
13. Emanuele, G.; Marco, P.; Fabio, C.; Matthias, N.; Francesco, C.; Francesco, G. Detection of stator turns short-circuit during sensorless operation by means of the Direct Flux Control technique. In Proceedings of the 2020 AEIT International Annual Conference (AEIT), Catania, Italy, 23–25 September 2020; pp. 1–6.
14. Pedrosa, D.; Carvalho, J.; Gonçalves, H.; Monteiro, V.; Fernandes, A.; Afonso, J.L. Field oriented control of an axial flux permanent magnet synchronous motor for traction solutions. In Proceedings of the IECON 2014—40th Annual Conference of the IEEE Industrial Electronics Society, Dallas, Texas, USA, 29 October 2014; pp. 1466–1472.
15. Sun, X.; Chen, L.; Yang, Z.; Zhu, H. Speed-sensorless vector control of a bearingless induction motor with artificial neural network inverse speed observer. *IEEE/ASME Trans. Mechatron.* **2012**, *18*, 1357–1366. [[CrossRef](#)]
16. Yang, Y.P.; Chuang, D.S. Optimal design and control of a wheel motor for electric passenger cars. *IEEE Trans. Magn.* **2006**, *43*, 51–61. [[CrossRef](#)]
17. Sun, X.; Su, B.; Wang, S.; Yang, Z.; Lei, G.; Zhu, J.; Guo, Y. Performance analysis of suspension force and torque in an ibpmsm with v-shaped pms for flywheel batteries. *IEEE Trans. Magn.* **2018**, *54*, 1–4. [[CrossRef](#)]
18. Sun, X.; Chen, L.; Jiang, H.; Yang, Z.; Chen, J.; Zhang, W. High-performance control for a bearingless permanent-magnet synchronous motor using neural network inverse scheme plus internal model controllers. *IEEE Trans. Ind. Electron.* **2016**, *63*, 3479–3488. [[CrossRef](#)]
19. Preindl, M.; Bolognani, S. Model predictive direct speed control with finite control set of pmsm drive systems. *IEEE Trans. Power Electron.* **2012**, *28*, 1007–1015. [[CrossRef](#)]
20. Boazzo, B.; Pellegrino, G. Model-based direct flux vector control of permanent-magnet synchronous motor drives. *IEEE Trans. Ind.* **2015**, *51*, 3126–3136. [[CrossRef](#)]
21. Siahbalaee, J.; Vaez-Zadeh, S.; Tahami, F. A new loss minimization approach with flux and torque ripples reduction of direct torque controlled permanent magnet synchronous motors. In Proceedings of the 2009 13th European Conference on Power Electronics and Applications, Barcelona, Spain, 8–10 September 2009; pp. 1–8.
22. Abdelrahem, M.; Zhang, Z.; Kennel, R.; Eldeeb, H.; Hackl, C. Simple and robust direct-model predictive current control technique for pmsgs in variable-speed wind turbines. In Proceedings of the 2017 IEEE International Symposium on Predictive Control of Electrical Drives and Power Electronics (PRECEDE), Pilsen, Czech Republic, 4–6 September 2017; pp. 1–6.
23. Gao, X.; Abdelrahem, M.; Hackl, C.M.; Zhang, Z.; Kennel, R. Direct predictive speed control with a sliding manifold term for pmsm drives. *IEEE J. Emerg. Sel. Top. Power Electron.* **2019**, *8*, 1258–1267. [[CrossRef](#)]
24. Abdelrahem, M.; Hackl, C.; Kennel, R.; Rodriguez, J. Sensorless predictive speed control of permanent-magnet synchronous generators in wind turbine applications In Proceedings of the PCIM Europe 2019, International Exhibition and Conference for Power Electronics, Intelligent Motion, Renewable Energy and Energy Management, VDE, Nuremberg, Germany, 7–9 May 2019; pp. 1–8.

25. Abdelrahem, M.; Hackl, C.; Kennel, R. Model predictive control of permanent magnet synchronous generators in variable-speed wind turbine systems. In Proceedings of the Power and Energy Student Summit (PESS 2016), Aachen, Germany, 19–20 January 2016.
26. Kiselev, A.; Kuznetsov, A. Motor drive control of a full-electric vehicle using generalized predictive control algorithm. In Proceedings of the 2014 IEEE International Electric Vehicle Conference (IEVC), Florence, Italy, 17–19 December 2014; pp. 1–5.
27. Rodriguez, J.; Cortes, P. *Predictive Control of Power Converters and Electrical Drives*; John Wiley & Sons: Hoboken, NJ, USA, 2012; Volume 40.
28. Cortés, P.; Kazmierkowski, M.P.; Kennel, R.M.; Quevedo, D.E.; Rodríguez, J. Predictive control in power electronics and drives. *IEEE Trans. Ind. Electron.* **2008**, *55*, 4312–4324. [[CrossRef](#)]
29. Hu, J.; Zhu, Z. Improved voltage-vector sequences on dead-beat predictive direct power control of reversible three-phase grid-connected voltage-source converters. *IEEE Trans. Power Electron.* **2012**, *28*, 254–267. [[CrossRef](#)]
30. Kang, J.; Li, X.; Liu, Y.; Mu, S.; Wang, S. Predictive current control with torque ripple minimization for pmsm of electric vehicles. In Proceedings of the 2018 IEEE International Power Electronics and Application Conference and Exposition (PEAC), Shenzhen, China, 4–7 November 2018; pp. 1–6.
31. Hackl, C.M. Mpc with analytical solution and integral error feedback for lti mimo systems and its application to current control of grid-connected power converters with lcl-filter. In Proceedings of the 2015 IEEE International Symposium on Predictive Control of Electrical Drives and Power Electronics (PRECEDE), Valparaiso, Chile, 5–6 October 2015; pp. 61–66.
32. Rodriguez, J.; Kazmierkowski, M.P.; Espinoza, J.R.; Zanchetta, P.; Abu-Rub, H.; Young, H.A.; Rojas, C.A. State of the art of finite control set model predictive control in power electronics. *IEEE Trans. Ind.* **2012**, *9*, 1003–1016. [[CrossRef](#)]
33. Garcia, C.; Rodriguez, J.; Odhano, S.; Zanchetta, P.; Davari, S.A. Modulated model predictive speed control for pmsm drives. In Proceedings of the 2018 IEEE International Conference on Electrical Systems for Aircraft, Railway, Ship Propulsion and Road Vehicles & International Transportation Electrification Conference (ESARS-ITEC), Nottingham, UK, 7–9 November 2018; pp. 1–6.
34. Van Ngo, B.Q.; Rodriguez-Ayerbe, P.; Olaru, S.; Model predictive control with two-step horizon for three-level neutral-point clamped inverter. In Proceedings of the 20th International Conference on Process Control (PC), Štrbské Pleso, Slovak Republic, 9–12 June 2015; pp. 215–220.
35. Vázquez Pérez, S.; Rodríguez, J.; Rivera, M.; García Franquelo, L.; Norambuena, M. Model predictive control for power converters and drives: Advances and trends. *IEEE Trans. Ind.* **2017**, *64*, 935–947. [[CrossRef](#)]
36. Zhang, Y.; Xie, W.; Li, Z.; Zhang, Y. Low-complexity model predictive power control: Double-vector-based approach. *IEEE Trans. Ind.* **2014**, *61*, 5871–5880. [[CrossRef](#)]
37. Riar, B.S.; Scoltock, J.; Madawala, U.K. Model predictive direct slope control for power converters. *IEEE Trans. Power Electron.* **2017**, *32*, 2278–2289. [[CrossRef](#)]
38. Zhang, Y.; Yang, H. Two-vector-based model predictive torque control without weighting factors for induction motor drives. *IEEE Trans. Power Electron.* **2016**, *31*, 1381–1390. [[CrossRef](#)]
39. Sheng, L.; Li, D.; Ji, Y. Two-vector fcs-mpc for permanent-magnet synchronous motors based on duty ratio optimization. *Math. Probl. Eng.* **2018**, *2018*, 9061979. [[CrossRef](#)]
40. Zhang, Y.; Gao, S.; Xu, W. An improved model predictive current control of permanent magnet synchronous motor drives. In Proceedings of the 2016 IEEE Applied Power Electronics Conference and Exposition (APEC), Long Beach, Canada, 20–24 March 2016; pp. 2868–2874.
41. J. Rodríguez, Kennel, R.M.; Espinoza, J.R.; Trincado, M.; Silva, C.A.; Rojas, C.A. High-performance control strategies for electrical drives: An experimental assessment. *IEEE Trans. Ind. Electron.* **2012**, *59*, 812–820. [[CrossRef](#)]
42. Abdelrahem, M.; Hackl, C.M.; Kennel, R.; Rodriguez, J. Efficient direct-model predictive control with discrete-time integral action for pmsg. *IEEE Trans. Energy Convers.* **2018**, *34*, 1063–1072. [[CrossRef](#)]
43. Zhang, Y.; Xu, D.; Liu, J.; Gao, S.; Xu, W. Performance improvement of model-predictive current control of permanent magnet synchronous motor drives. *IEEE Trans. Ind. Appl.* **2017**, *53*, 3683–3695. [[CrossRef](#)]
44. Vazquez, S.; Leon, J.I.; Franquelo, L.; Carrasco, J.; Martinez, O.; Rodriguez, J.; Cortes, P.; Kouro, S. Model predictive control with constant switching frequency using a discrete space vector modulation with virtual state vectors. In Proceedings of the 2009 IEEE International Conference on Industrial Technology, Churchill, VIC, Australia, 10–13 February 2009; pp. 1–6.
45. Zhang, Y.; Bai, Y.; Yang, H. A universal multiple-vector-based model predictive control of induction motor drives. *IEEE Trans. Power Electron.* **2017**, *33*, 6957–6969. [[CrossRef](#)]
46. Habibullah, M.; Lu, D.D.C.; Xiao, D.; Rahman, M.F. A simplified finite-state predictive direct torque control for induction motor drive. *IEEE Trans. Ind. Electron.* **2016**, *63*, 3964–3975. [[CrossRef](#)]
47. I.M.-Hassine, B.; Naouar, M.W.; Mrabet-Bellaaj, N. Model predictive-sliding mode control for three-phase grid-connected converters. *IEEE Trans. Ind. Electron.* **2017**, *64*, 1341–1349. [[CrossRef](#)]
48. Zhang, Y.; Xu, D.; Huang, L. Generalized multiple-vector-based model predictive control for pmsm drives. *IEEE Trans. Ind. Electron.* **2018**, *65*, 9356–9366. [[CrossRef](#)]
49. Xie, W.; Wang, X.; Wang, F.; Xu, W.; Kennel, R.; Gerling, D.; Lorenz, R. Finite-control-set model predictive torque control with a deadbeat solution for PMSM drives. *IEEE Trans. Ind. Electron.* **2015**, *62*, 5402–5410. [[CrossRef](#)]
50. Zhang, X.; Hou, B. Double vectors model predictive torque control without weighting factor based on voltage tracking error. *IEEE Trans. Power Electron.* **2018**, *33*, 2368–2380. [[CrossRef](#)]

51. Zhang, X.; He, Y. Direct voltage-selection based model predictive direct speed control for PMSM drives without weighting factor. *IEEE Trans. Power Electron.* **2019**, *34*, 7838–7851. [[CrossRef](#)]
52. Wang, Y.; Wang, X.; Xie, W.; Wang, F.; Dou, M.; Kennel, R.; Lorenz, R.D.; Gerling, D. Deadbeat model-predictive torque control with discrete space-vector modulation for PMSM drives. *IEEE Trans. Ind. Electron.* **2017**, *64*, 3537–3547. [[CrossRef](#)]
53. Abdelrahem, M.; Rodríguez, J.; Kennel, R. Improved Direct Model Predictive Control for Grid-Connected Power Converters. *Energies* **2020**, *13*, 2597. [[CrossRef](#)]
54. Bouguenna, I.F.; Azaiz, A.; Tahour, A.; Larbaoui, A. Robust neuro-fuzzy sliding mode control with extended state observer for an electric drive system. *Energy* **2019**, *169*, 1054–1063. [[CrossRef](#)]
55. Singh, B.; Goyal, D. Improved dsvm-dtc based current sensorless permanent magnet synchronous motor drive. In Proceedings of the 2007 7th International Conference on Power Electronics and Drive Systems, Bangkok, Thailand, 27–30 November 2007; pp. 1354–1360.
56. Sun, Y.; Zhai, S.; Cui, H.; Nan, D.; Wang, K. Frequency regulation strategy for private evs participating in integrated power system of res considering adaptive markov transition probability. *Electr. Power Syst. Res.* **2019**, *173*, 291–301. [[CrossRef](#)]
57. Mansour, M.; Mansouri, M.; Bendoukha, S.; Mimouni, M. A grid-connected variable-speed wind generator driving a fuzzy-controlled pmsg and associated to a flywheel energy storage system. *Electr. Power Syst. Res.* **2020**, *180*, 106137. [[CrossRef](#)]
58. Maamoun, A.; Alsayed, Y.; Shaltout, A. Fuzzy logic based speed controller for permanent-magnet synchronous motor drive. In Proceedings of the 2013 IEEE International Conference on Mechatronics and Automation, Takamatsu, Japan, 4–7 August 2013; pp. 1518–1522.
59. Rashid, G.; Ali, M.H. Fault ride through capability improvement of dfig based wind farm by fuzzy logic controlled parallel resonance fault current limiter. *Electr. Power Syst. Res.* **2017**, *146*, 1–8. [[CrossRef](#)]
60. Faddel, S.; Mohamed, A.A.; Mohammed, O.A. Fuzzy logic-based autonomous controller for electric vehicles charging under different conditions in residential distribution systems. *Electr. Power Syst. Res.* **2017**, *148*, 48–58. [[CrossRef](#)]
61. Bouzeria, H.; Fetha, C.; Bahi, T.; Abadlia, I.; Layate, Z.; Lekhchine, S. Fuzzy logic space vector direct torque control of pmsm for photovoltaic water pumping system. *Energy Procedia* **2015**, *74*, 760–771. [[CrossRef](#)]